Korean J. Chem. Eng., 34(1), 259-265 (2017)
DOI: 10.1007/s11814-016-0231-2

pISSN: 0256-1115
eISSN: 1975-7220

High performance methyl orange capture on magnetic nanoporous MCM-41 prepared by incipient wetness impregnation method

Talib Mohammed Albayati†, Ghanim Magbol Alwan, and Omar Sabah Mahdy

Department of Chemical Engineering, University of Technology, 52 Alsinaa St., P. O. Box 35010, Baghdad, Iraq
(*Received 2 May 2016 • accepted 11 August 2016*)

Abstract−The Magnetic nanoporous material Fe/MCM-41 was prepared, and its physical characterization studied, to determine the effect of its properties on separation efficiency of methyl orange (MO) from wastewater by adsorption process. The experimental results were analyzed for both adsorbent mesoporous material samples, MCM-41 and magnetic Fe/MCM-41, in order to select the best operating conditions for the different studied parameters, which are: constant temperature (20 °C), pH: (2) adsorbent dosage (0.03 gm), contact time (10 minute) and concentrations (30 mg/L). The results demonstrate that the adsorption processes can be well fitted by the Langmuir isotherm model for pure MCM-41, with a correlation coefficient of (0.999), and fitted by the Freundlich isotherm model for magnetic Fe/MCM-41, with a correlation coefficient of (0.994). The adsorption kinetics of MO on to MCM-41 and Fe/MCM-41 are well described by a pseudo-second-order kinetic model.

Keywords: Separation, Wastewater, MCM-41, Methyl Orange, Adsorption

INTRODUCTION

Synthetic dyes with complex aromatic structures are commonly used in numerous industries, including the manufacture of textile, leather, printing, and food, plastic and pharmaceutical products. These dyes are organic materials that contain complex chemical compounds that are stable in certain temperature, light, and oxidizing environments, and in these environments they are not biodegradable [1].

Methyl orange (MO) [$C_{14}H_{14}N_3SO_3Na$] is one of the most common dyes. Its chemical formula and molecular composition are depicted in Fig. 1. MO can be used as both a pH indicator for titrations or as dye for many industries. It can be synthesized by the interaction of dimethylanilin, sulfanilic acid, and sodium nitrite. The IUPAC name for MO is 4-dimethylaminoazobenzene-4′-sulfonic acid sodium salt.

Dye pollution can be minimized by chemical, physical and biological processes, such as through chemical oxidation, coagulation, filtration and membrane separation, or microbial degradation [2]. However, these methods have their difficulties and limitations, including the possible generation of secondary pollutants, a high cost of use, and low removal efficiency. Adsorption process has been established as an alternative method with high potential for the removal of dyes from wastewater, and the adsorbent most commonly used is activated carbon [3-7]. The use of activated carbon has many disadvantages, though [8]. It is quite expensive, and is ineffective and non-selective against disperse and vat dyes [9]. This has driven many to search for more effective and economic sorbents as potential replacements for activated carbon.

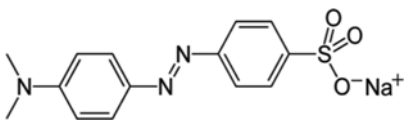

Fig. 1. Molecular structure of methyl orange.

Recently, magnetic nanoporous silicas have generated much interest in the combined use of mesoporous structure with appropriate magnetization [10,11]. Such a combination allows separation remediation to be brought about in liquid-phase processes by the implementation of an external magnetic field. The magnetic characteristics for nanoporous materials suggest fantastic prospects for their use in different fields, including sorption, catalysis, photonics, separation, and drug delivery, and as components in electronic devices. For separation applications, it is necessary to prepare such magnetic nanoporous materials with tunable shell thickness and controllable surface area for adsorption [12-15].

This study focuses on the preparation and characterization of mesoporous silicate nanocomposite magnetic Fe/MCM-41, consisting of magnetic Fe_2O_3 nanoparticles scattered inside pores of mesoporous MCM-41, and its implementation in the separation of organic MO dye from wastewater. The effects of pH solution, adsorbent dosage, MO concentration, and contact time on removal efficiency and adsorption capacity were also investigated. The magnetic Fe_2O_3 precursor Fe $(NO_3)_3{\cdot}9H_2O$ was loaded onto the mesoporous support MCM-41 by using the incipient wetness impregnation method. The use of MO was prompted by its positive charge in solution. Furthermore, the orange color of MO allows easy visualization and spectrophotometric observation of the system during separation experiments. The novelty of this study is relating to the application of a nanoporous MCM-41 as a magnetic adsorbent for removal of methyl orange (MO) dye pollutants from

†To whom correspondence should be addressed.
E-mail: talib_albyati@yahoo.com

wastewater in batch adsorption system, due to their high specific surface areas, pore volumes and attractive sites.

MATERIALS AND METHODS

1. Chemicals

Tetraethyl orthosilicate (TEOS, 98%), sodium hydroxide (NaOH), cetyltrimethyl ammonium bromide (CTAB, 99%), methyl orange (MO) [$C_{14}H_{14}N_3SO_3Na$] and ethanol (EtOH, 99%) were purchased from Sigma Aldrich. Ferric nitrate hidrate (Fe $(NO_3)_3 \cdot 9H_2O$, 98%) was purchased from Alpha Chemika (Made in India). All chemicals were used as received without further purification.

2. Preparation of MCM-41 Mesoporous

The source of silica was CTAB and TEOS, respectively. MCM-41 was synthesized by adding 5.78 g of TEOS (27.7 mmol) into a solution containing 1.01 g of CTAB (2.8 mmol) and 0.34 g of NaOH (8.5 mmol) in 30 mL of de-ionized water [16]. After stirring for 1 h at ambient temperature, the resulting homogeneous mixture was crystallized under static hydrothermal conditions at 110 °C in a Teflon bottle for 96 h. The solid product was obtained by filtration, washed with de-ionized water, ethanol and dichloromethane, and then dried in air at room temperature.

3. Preparation of Nanosized Magnetic Fe/MCM- 41

The MCM-41 sample was metal-loaded using incipient wetness impregnation (IWI), with Fe $(NO_3)_3 \cdot 9H_2O$ as the iron source [17]. Impregnation solution was synthesized by dissolving a convenient quantity of metals (1% loading) into H_2O solvent to load the Ferric with a 1 wt%. To obtain a high metal dispersion and prevent conglomeration of the salt during the vaporization of the solvent, the volume of the loaded metal solution was equal to that of the used pore volume of the support. After impregnation, the adsorbent was dried overnight in air at room temperature, then for 24 h at 120 °C, and lastly calcined at 500 °C for 4 h to get the 1% Fe/MCM-41 magnetic adsorbents.

4. Characterization

XRD patterns were recorded under ambient conditions on MiniFlex (Rigaku) with Cu Kα radiation (λ=1.5406 Å). The X-ray tube was activated at 40 kV and 30 mA while the diffractometer was set to record in the 2θ range of 0.5-8° with a 2θ step size of 0.01 and a step time of 10 s. The unit cell and d-spacing parameters were calculated using $n\lambda=2d\sin\theta$ and $a_o=2d100/\sqrt{3}$. HORIBA surface area analysis (SA-9600 Series) was conducted for nitrogen adsorption/desorption measurements. The samples were degassed for 3 h at 350 °C under vacuum (p<5-10 mbar) in the degas port of the sorption analyzer. Brunauer-Emmett-Teller (BET) method was followed to calculate the BET specific surface areas of the samples in the range of relative pressures between 0.05 and 0.35. The total pore volume was specified from the adsorption branch of the N_2 isotherm as the amount of liquid nitrogen adsorbed at P/Po=0.995. The pore wall thickness (Wt) was estimated from the unit cell parameter (a_o) and pore size diameter (dP). Mean mesopore diameters for the various samples were calculated from the nitrogen sorption data using BET analysis (4V/A). The macropore structure was characterized by scanning electron microscopy (SEM), performed on a TE SCAN (Model VEGA III). The (FT- IR) infrared spectra of the powder samples were diluted in (8 wt%) KBr and recorded at ambient condition in transmission mode in the range of 4,000 to 400 cm^{-1} at 4 cm^{-1} resolution regions using a NICOLET 380 FT-IR spectrometer.

5. Preparation of Adsorbate Solution

The stock solution was prepared by dissolving 1 g of MO in distilled water making a 1,000 ml stock solution in a volumetric flask. From the stock, different concentrations (10-50 mg/*l*) of MO were prepared by diluting with distilled water.

6. Batch Adsorption

Experiments were designed to evaluate MO adsorption isotherms over the adsorbents at 25 °C. The MO molecule was prepared by 1 g dissolved in 1 L of distilled water. A calibration curve was then constructed from ten concentrations (0-1 g/L) of the methyl orange stock solution by using a UV-Spectrophotometer (HP 8453) set at 25 °C. The λ max was found to be 464 nm. The calibration was fundamental to obtaining the comparison of final adsorbance to initial adsorbance. An amount of 0.01 g MCM-41 and magnetic Fe/MCM-41 was added to 100 ml of MO solution, and then placed on a shaker (Unimax 1010 DT Heidolph) at 150 rpm and ambient condition (25 °C) for 1 h.

The different studied parameters were included for both adsorbent mesoporous material, MCM-41 and magnetic Fe/MCM-41: **(i)** effect of pH: (2-10) at a constant temperature (20 °C), adsorbent dosage (0.05 g), contact time (50 min), and concentrations (50 mg/L); **(ii)** effect of adsorbent dosage: (0.01-0.05 g) at a constant temperature (20 °C), pH adjusted at (2), contact time (50 min), and concentrations (50 mg/L); **(iii)** effect of MO concentration: (10-50 mg/L) at a constant temperature (20 °C), pH adjusted at (2), adsorbent dosage (0.03 gm), and contact time (50 min); **(iv)** effect of contact time: (10-50 min) at a constant temperature (20 °C), pH adjusted at (2), adsorbent dosage (0.03 gm), and concentrations (30 mg/L).

Equal volumes of the solutions were filtered at the end of the adsorption process by filter paper (U-01, 15 cm×100 circles) to allow the adsorbent mesoporous material, both MCM-41 and magnetic Fe/MCM-41, to completely separate from the solution. The analysis was achieved by using a UV-spectrophotometer (TU1900) at a wavelength of 464 nm. The removal percentage (R) of MO solution was estimated by the following equation:

$$\%R = \frac{Co - Ce}{Co} \times 100\% \quad (1)$$

where Co (mg/L) and Ce (mg/L) are the initial and equilibrium liquid-phase concentration of MO, respectively.

7. Adsorption Isotherm Model

The Langmuir and Freundlich isotherm equations were fitted to the adsorption data for MO. The Langmuir linearization form equation [18] is as follows:

$$\frac{C_{eq}}{q_e} = \frac{1}{q_m} C_{eq} + \frac{1}{K_L q_m} \quad (2)$$

where, q_m (mg/g) is the Langmuir constant relating to adsorption capacity. K_L is the constant that refers to energy of adsorption (L/mg). The constants q_m and K_L could be specified from a linearization form of Eq. (3) by the slope of the linear plot of C_{eq}/q_e versus C_{eq}.

The dimensionless equilibrium parameter R_L is defined as follows [19]:

$$R_L = \frac{1}{1+K_L C_0} \quad (3)$$

where K_L is the Langmuir constant (L/mg) and C_0 is the highest initial dye concentration (mg/L). This parameter shows the isotherm is favorable (R_L<1), unfavorable (R_L>1), irreversible (R_L=0), or linear (R_L=1) [20]. The Freundlich linear form equation is given by [21,22]:

$$\ln q_e = \ln K_f + \frac{1}{n}\ln C_{eq} \quad (4)$$

where; ln and K_f are Freundlich constants related to adsorption intensity and adsorption capacity, respectively, of the sorbent. The values of ln and K_f can be obtained from the slope and intercept, respectively, of the linear plot of experimental data of $\ln q_e$ versus $\ln C_{eq}$.

RESULTS AND DISCUSSION

1. Characterization of Adsorbents

XRD patterns of MCM-41 and Fe/MCM-41 samples are illustrated in Fig. 2, which shows an intense diffraction peak (1 0 0) at about 2θ of 2.53° for MCM-41 and 2.56° for 1% Fe/MCM-41. Furthermore, two extra peaks were seen in the XRD patterns, which could be indicated as (2 1 1) and (2 2 0). A series of weak peaks in the range 3.5°-5.5° indicate Ia3d cubic structure. The peaks observed correspond closely to the same peaks recorded in the literature [23,24].

The clarification of SEM for pure MCM-41 and magnetic Fe/MCM-41 is presented in (Fig. 3(a) and (b)) and (Fig. 3(c) and (d)), respectively. The images reveal that all samples represent a highly crystalline material with clearly visible cubic crystals before and after impregnation with Fe $(NO_3)_3 \cdot 9H_2O$. This implies that Fe was smoothly scattered on the surface, inserted in the pore walls, or inside the hexagonal channels of MCM-41. Indeed, SEM studies with different magnifications proved that 1% Fe/MCM-41 magnetic adsorbents showed good dispersion of homogenous particles [25].

The BET surface area, pore volume, pore diameter, and real density of pure MCM-41 and magnetic Fe/MCM-41 samples were measured and summarized in Table 1. These results show that the prepared pure mesoporous material MCM-41, with higher surface area and pore volume, falls within the range of surface area (1,000-1,500 m^2g^{-1}) and pore volume (0.4-0.9 cm^3/g) for MCM-41

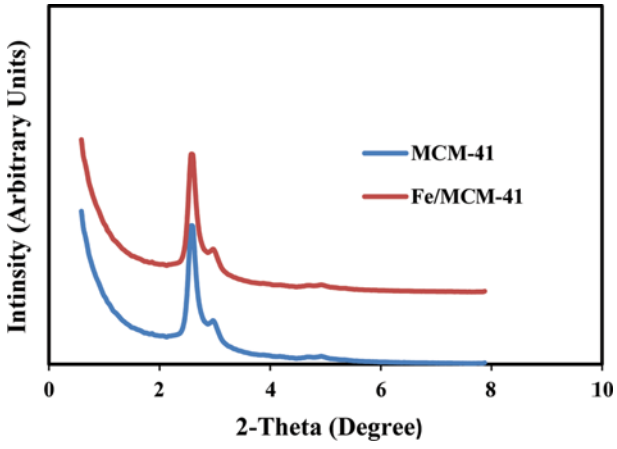

Fig. 2. XRD patterns of pure MCM-41 and magnetic Fe/MCM-41 samples.

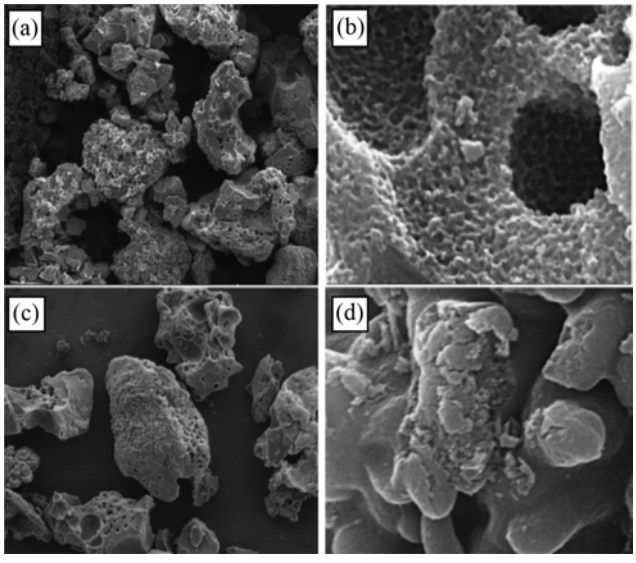

Fig. 3. (a) And (b) SEM image of pure MCM-41 (c) and (d) SEM image of magnetic Fe/MCM-41.

Table 1. The Structure properties of nanoporous material SBA-15

Material	d_{100}[a] (nm)	a_o[b] (nm)	D_p[c] (nm)	W_t[d] (nm)	P_V[e] (cm^3/g)	S_{BET}[f] (m^2/g)	μ_p[g] (cm^3/g)
MCM-41	3.48	4.02	3.28	0.74	0..94	1450.9	0.132
Fe/MCM-41	3.44	3.98	2.84	1.14	0.41	1216.2	0.053

[a]d-Spacing of (100) reflection
[b]Unit cell constant, $a_o = 2d100/\sqrt{3}$
[c]Average pore diameter, estimated using the desorption branch of the isotherm and the Barrett-Joyner-Halenda (BJH) method
[d]The pore wall thickness estimated from the difference (a_o _ Dp)
[e]Total pore volume, taken from the volume of N2 adsorbed at p/p_0=0.95
[f]BET surface area, calculated from the linear part of the BET plot
[g]Micro pore volume

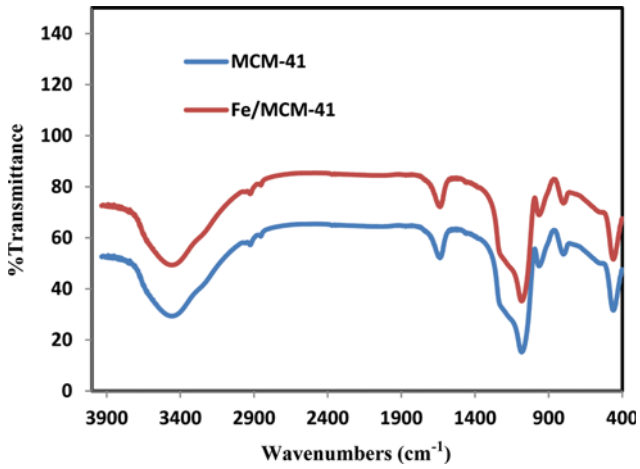

Fig. 4. FT-IR spectra of pure MCM-41 and magnetic Fe/MCM-41.

and Fe/MCM-41 [26].

Fig. 4 shows the FTIR spectra of the pure MCM-41 and magnetic Fe/MCM-41 samples. The Si OH broad bands are between 3,700 and 2,900 cm^{-1}, and a strong absorption band centered at 1,630 cm^{-1} is observed for both samples. Moreover, the obviously enhanced intensity of the above two bands for MCM-41 and magnetic Fe/MCM-41 suggests the presence of a higher amount of metallic ions in the silica framework. The two samples have the characteristic bands for Si O Si at 799, 1050, 1,200, and 1,250 cm^{-1}, and the Si OH bands at 940 and 3,463 cm^{-1}. The Si OH band of MCM-41 and Fe/MCM-41 at 3,740 cm^{-1} decreased after grafting. Additional bands belonging to H O H (1,630 cm^{-1}), stretching (1,100 cm^{-1}), and Si O Si (790 cm^{-1}) are prominent in MCM-41 and Fe/MCM-41 [27,28].

2. Adsorption of MO

2-1. Effect of pH

pH is one of the important variables that influence adsorption process. It affects not only the surface charge of the adsorbent, but also the ionization degree of the adsorbate. The experiments for removal of MO were achieved at different pHs, ranging between 2 and 10, and the results are illustrated in Fig. 5. The pH was adjusted with 0.1 N of HCl and NaOH solution. From Fig. 5, note that MO adsorption reduced when pH increased from 2 to 10. The removal efficiency increased in acidic pH but remained almost constant or decreased in basic conditions. The observed high adsorption of MO onto pure MCM-1 and magnetic Fe/MCM-41 at pH<4 is possibly due to the existence of surplus and negative (OH^-) ions competing with the MO positive charge group Na^+ for adsorption sites, causing an increase in the amount of MO adsorbed. However, when pH decreased, the surface of pure MCM-1 and magnetic Fe/MCM-41 became negatively charged, and the binding of positively charged dyes onto these surfaces became much more favorable, resulting in enhanced adsorption of dye [29]. The important conclusion of this figure is that there was no difference between pure MCM-41 and magnetic Fe/MCM-41in removal capacity. Removal of MO was 92% with pure MCM-41 and 96.7% with Fe/MCM-41. This result means that the dispersal of Fe particles into the pores of MCM-41 does not improve removal efficiency of MO when compared with pure MCM-41.

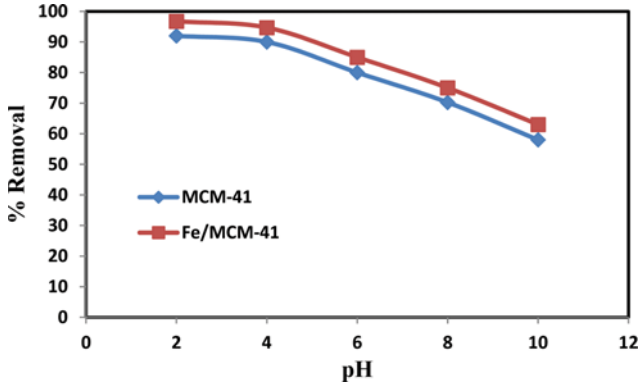

Fig. 5. Effect of pH on the removal of MO (C_o=50 mg/L, contact time=50 min, MCM-41 and Fe/MCM-41 dosage=0.05 g).

2-2. Effect of Adsorbent Dosage

The variation influence of the adsorbent mass for the pure MCM-41 and magnetic Fe/MCM-41 was conducted by increasing the adsorbent dosage from 0.01 g/50 mL to 0.05 g/50 mL for both adsorbents respectively, as shown in Fig. 6. Initial MO concentration was 50 mg/L. It was noted, for pure adsorbent MCM-41, and for magnetic adsorbent Fe/MCM-41, the removal percentage varied from 22.5% to 91% and from 32% to 95%, respectively. From this, it can be seen that removal efficiency grows with increase in adsorbent dosage for both adsorbents. This increase in MO removal efficiency could be attributed to the greater number of obtainable adsorption sites resulting from the increase in adsorbent [30,31].

The results show that adsorption capacity increases with increasing MCM-41 and Fe/MCM-41 dosage at a constant concentration of MO, until equilibrium is reached at 0.03 g/mL, which is considered the best adsorbent dose. The equilibrium in the removal efficiency is basically due to the driving force of MO molecules, which decrease with an increasing dosage of adsorbents, leading to high surface area, greater pore volume, and a larger number of adsorption sites [32]. From Fig. 6, the removal efficiency between

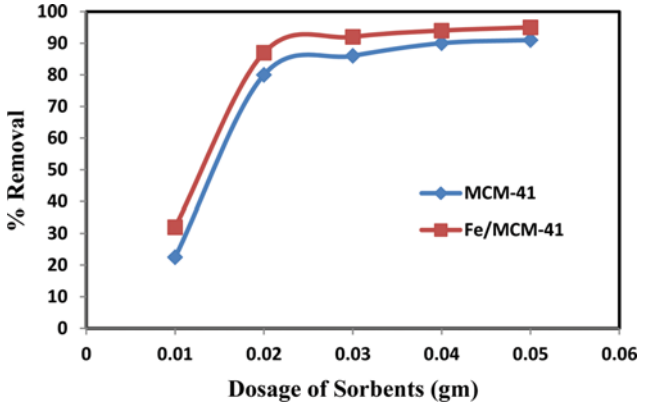

Fig. 6. Effect of adsorbent dose MCM-41 and Fe/MCM-41 on the removal efficiency of MO (C_o=50 mg/L, pH=2, contact time=50 min).

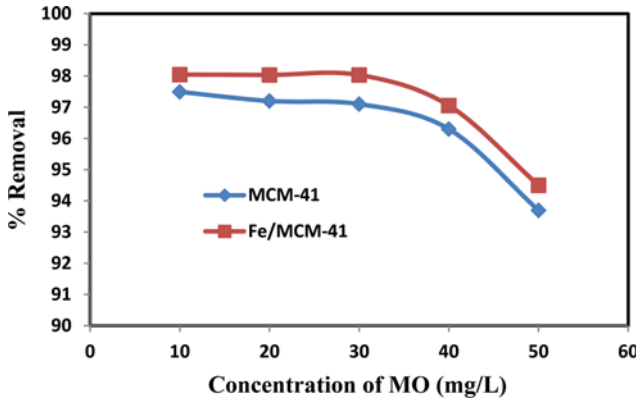

Fig. 7. Effect of initial MO concentration on removal efficiency (pH= 2, contact time=50 min, MCM-41 and Fe/MCM-41 dosage= 0.03 g).

the two adsorbents is only 4%, which is not significant. The difference may be caused by the dispersal of Fe particles into the pores of MCM-41, leading to a decrease in the surface area of the magnetic adsorbents Fe/MCM-41, as shown in Table 1.

2-3. Effect of Initial MO Concentration

The influence of initial MO concentration was studied by changing concentrations from 10 mg/L to 50 mg/L, as illustrated in Fig. 7. Removal efficiency decreased with increasing concentration of MO from 10 to 50 mg/L, due to the increase in the ratio of the dye's anion to the dosage of the adsorbent. As the number of effective adsorption sites required accommodating the remaining adsorbate increases, removal efficiency of adsorption decreases. With minimum concentrations of MO, the initial ratio of dye molecules to obtainable adsorption sites is low, and more adsorption sites are available for dye molecules, thus increasing the removal percentage [33].

Fig. 7 shows that the adsorption capacity of the magnetic nanocomposite adsorbent Fe/MCM-41 increased slightly compared with the pure adsorbent nanoporous material MCM-41 for the same MO concentration. Protonation dispersion of Fe particles into MCM-41 pores was unable to improve the adsorption of anion dye onto Fe/MCM-41 effectively.

2-4. Effect of Contact Time

The influence of contact time on the removal efficiency of MO was studied at an initial concentration of MB (C_o=30 mg/L, pH= 2, MCM-41 and Fe/MCM-41 dosage=0.03 g) as shown in Fig. 8. This figure illustrates that the removal efficiency of MO is very rapid in the first ten minutes of contact time, and that after 20 min, removal does not vary significantly. This could be due to the simple fact that a considerable number of unoccupied surface sites are available for adsorption at the beginning of contact. As the dye molecules fill the surface sites, fewer and fewer are left unoccupied, so that, at the end of the adsorption process, removal efficiency remains almost constant [34].

These results explain how the existence of Fe particles did not increase the 98% removal percentage of MO onto composite nanoporous material Fe/MCM-41 within 20 minutes of contact time, which is the same result for removal of MO by pure MCM-41. It can be concluded that the existence of magnetic nanoporous material did not improve removal efficiency of MO because Fe particles encapsulated in the pores of the MCM-41 adsorbent surface progressively blocked those pores and reduced the surface area of the adsorbent.

2-5. Selecting of Operating Conditions

The best removal for MO adsorbate by the two types of adsorbents MCM-41 and Fe/MCm-41 is illustrated in Fig. 9. Optimum operating conditions for different studied parameters were obtained for maximum removal efficiency for MO for both adsorbent mesoporous material samples, MCM-41 and magnetic Fe/MCM-41. The optimum operating conditions are: constant temperature (20 °C), pH (2), adsorbent dosage (0.03 g), contact time (10 minutes), and concentration (30 mg/L).

2-6. Adsorption Isotherms Model

Adsorption isotherms of MO on pure MCM-41 and magnetic Fe/MCM-41 are illustrated in Figs. 10 and 11, respectively. As the two figures show, uptake is maximized with equilibrium of MO dye concentrations in the range of empirical concentration. This is due to maximization of the driving force of the concentration gradient. When the concentration of MO in solution is higher, the active sites of MCM-41 and Fe/MCM-41 are surrounded by much more MO ions, and the process of adsorption maximizes. Therefore, the values of q_e are maximized with the equilibrium of MO concentrations.

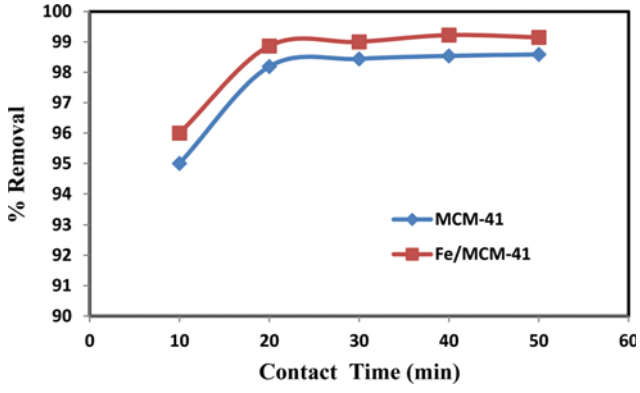

Fig. 8. Effect of contact time on the removal efficiency of MO (C_o= 30 mg/*l*, pH=2, MCM-41 and Fe/MCM-41 dosage=0.03 g).

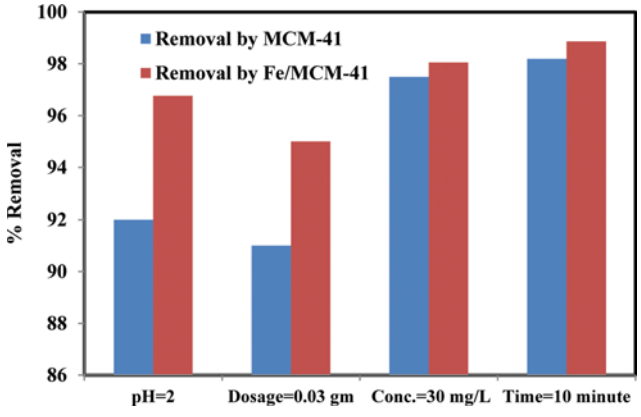

Fig. 9. The removal efficiency for MO at the best parameters conditions.

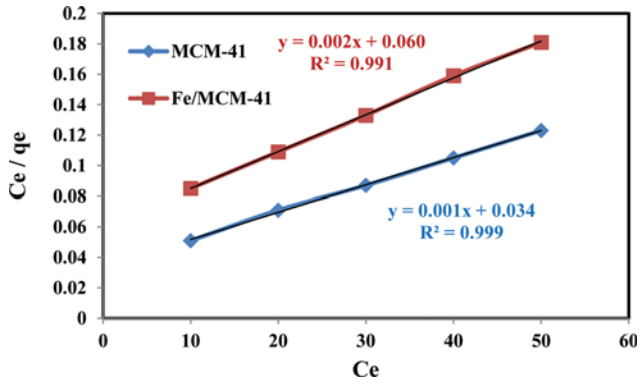

Fig. 10. Langmuir Isotherm model.

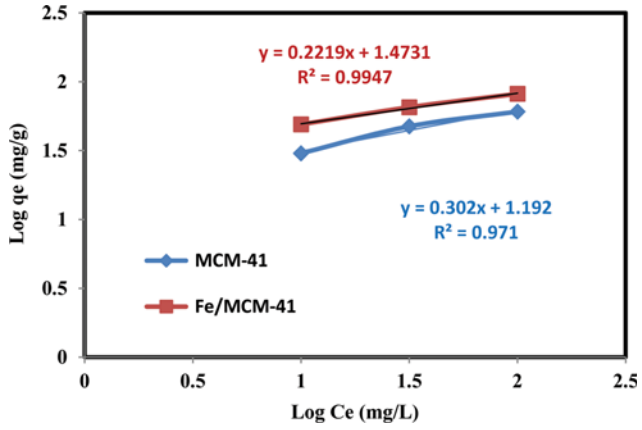

Fig. 11. Freundlich Isotherm model.

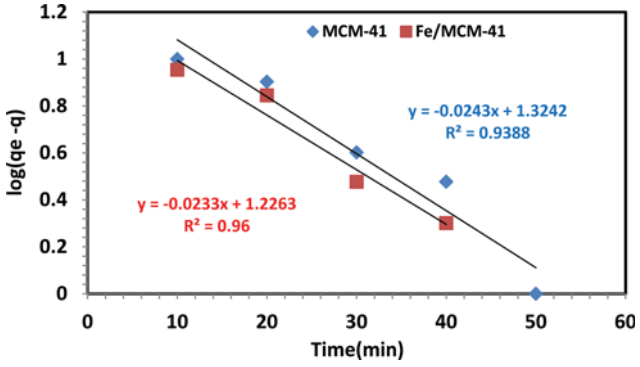

Fig. 12. Pseudo-first order kinetics models.

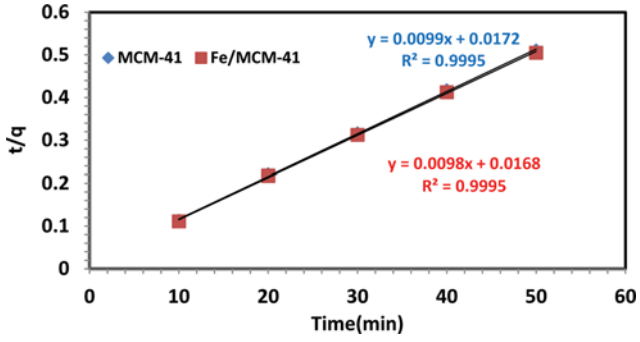

Fig. 13. Pseudo- second order kinetics models.

The linearized Langmuir and Freundlich plots results are given in Table 2, which shows the isotherm constants and R^2 correlation coefficient values for each model. The correlation coefficient values for the Langmuir isotherm model of MCM-41 and Fe/MCM-41 are (0.999 and 0.991), respectively. The values for the Freundlich isotherm model of MCM-41 and Fe/MCM-41 are (0.971 and 0.994), respectively. These values indicate that the Langmuir isotherm has a higher correlation coefficient for pure MCM-41 when compared with the Freundlich isotherm model, and vice versa for Fe/MCM-41. From this, it can be concluded that both adsorbents show a better fitting model with experimental data [35].

Table 2 also shows R_L values between 0 and 1, which reference adsorption of MO onto MCM-41 and Fe/MCM-41, and is favorable. Values of n less than 1 represent poor adsorption characteristics, those in the range of 1-2 represent moderate adsorption, and 2-10 represent good [36].

2-7. Adsorption Kinetics

The rate of MO adsorption by MCM-41and Fe/MCM-41 is one of the significant factors that define the efficiency of adsorption. The kinetics of the MO sorption on MCM-41and Fe/MCM-41 was examined by using pseudo-first and pseudo-second-order kinetics models as shown in Figs. 12 and 13. The parameters val-

Table 2. Isotherm parameters for MO adsorbed onto MCM-41 and Fe/MCM-41 with the correlation coefficient

Isotherms	Langmuir				Freundlich		
	q_{max} (mg/g)	K_L (L/mg)	R^2	R_L	K_F (L/g)	1/n	R^2
MCM-41	1000	0.029	0.999	0.408	0.0765	0.302	0.971
Fe/MCM-41	500	0.033	0.991	0.377	0.168	0.221	0.994

Table 3. Kinetic adsorption parameters obtained by using pseudo-first order and pseudo-second order models for MCM-41 and Fe/MCM-41

Adsorbents	Pseudo-first order				Pseudo-second order		
	q_e (exp.) mg/g	q_e (cal.) mg/g	k_1 min^{-1}	R^2	q_e (cal.) mg/g	k_2 g/mg·min	R^2
MCM-41	98	21.1	0.055963	0.9388	101	0.005698	0.9995
F-MCM-41	99	16.83	0.05366	0.96	102	0.005717	0.9995

ues of the kinetic models and the correlation coefficients (R^2) are listed in Table 3. The theoretical (q_e *cal.*) values estimated from the pseudo-first-order kinetic model gave significantly different value compared to experimental (q_e *exp.*) value**,** as shown in Table 3; therefore, the pseudo-first-order kinetic model did not describe well this adsorption system. While**,** Table 3 shows the theoretical (q_e *cal.*) values, estimated from the pseudo-second order kinetic model, are very close to the experimental (q_e *cal.*) value. Furthermore, the coefficients R^2 value is close to 1, confirming the applicability of the pseudo-second-order equation for MCM-41and Fe/MCM-41; therefore, Fig. 13 shows superposition for both samples [36].

CONCLUSION

MCM-41 was prepared by conventional method and grafted with Fe to create magnetic Fe/MCM-41 using the incipient wetness impregnation (IWI) method. Maximum removal for both adsorbent mesoporous material samples, MCM-41 and Fe/MCM-41, was obtained in a batch adsorption system at 20 °C, pH of 2, adsorbent dosage of 0.03 gm, contact time of 10 minutes, and concentration of 30 mg/L.

The obtained Fe/MCM-41 displayed high activity in the separation of MO. Magnetic Fe/MCM-41 created by the IWI method demonstrated adsorbent activity similar to that prepared by traditional method, although magnetic Fe/MCM-41 adsorbents have the advantage of good adsorbent recovery of the MO. The results show that, at room temperature, MO can be separated at the same rate on the surface and pore channels of both pure MCM-41 and Fe/MCM-41.

The adsorption isotherm studies demonstrate that the adsorption process is well fitted by the Langmuir isotherm model for pure MCM-41, with a higher correlation coefficient 0.999, and by the Freundlich isotherm model for magnetic Fe/MCM-41, with a higher correlation coefficient 0.994. The adsorption kinetics of MO onto MCM-41 and Fe/MCM-41 are well described by a pseudo-second-order kinetic model.

ACKNOWLEDGEMENTS

We gratefully acknowledge financial support from the Department of Chemical Engineering, University of Technology/Baghdad, Iraq.

REFERENCES

1. A. Rodríguez, J. García, G. Ovejero and M. Mestanza, *J. Hazard. Mater.*, **172**, 1311 (2012).
2. E. Forgacs, T. Cserháti and G. Oros, *Environ. Int.*, **30**, 953 (2009).
3. Q. F. Alsalhy, T. M. Albyati and M. A. Zablouk, *Chem. Eng. Commun.*, **200**(1), 1 (2013).
4. T. M. Albayati and A. M. Doyle, *Adsorpt. Sci. Technol.*, **31**(5), 459 (2013).
5. T. M. Albayati and A. M. Doyle., *Chem.: Bulgarian J. Sci. Education*, **23**(1), 105 (2014).
6. T. M. Albayati, *Part. Sci. Technol.*, **32**(6), 616 (2014).
7. A. A. Sabri, T. M. Albayati and R. A. Alazawi, *Korean J. Chem. Eng.*, **32**(9), 1835 (2015).
8. S. Babel and T. A. Kurniawan, *J. Hazard. Mater.*, **97**, 219 (2003).
9. V. K. Gupta, *J. Environ. Manage.*, **90**, 2313 (2009).
10. A. H. Lu, W. C. Li., A. Kiefer, W. Schmidt, E. Bill, G. Fink and F. Schuth, *J. Am. Chem. Soc.*, **126**, 8616 (2004).
11. P. Wu, J. Zhu and Z. Xu, *Adv. Funct. Mater.*, **14**, 345 (2004).
12. S. Huang, P. Yang, Z. Cheng, C. Li., Y. Fan, D. Kong and J. Lin, *J. Phys. Chem. C*, **112**, 7130 (2008).
13. S. Giri, B. G. Trewyn, M. P. Stellmaker and V. S. Lin, *Angew. Chem. Int. Ed.*, **44**, 5038 (2005).
14. Y. Deng, D. Qi, C. Deng, X. Zhang and D. Zhao, *J. Am. Chem. Soc.*, **130**, 28 (2008).
15. Y. Xingbin, C. Jiangtao, X. Qunji and M. Philippe, *Micropor. Mesopor. Mater.*, **135**, 137 (2010).
16. H. Chen and Y. Wang, *Ceram. Int.*, **28**, 541 (2002).
17. T. M. Albayati and A. M. Doyle, *J. Nanopart. Res.*, **17**(2), 109 (2015).
18. I. Langmuir, *J. Am. Chem. Soc.*, **38**(11), 2221 (1916).
19. W. J. Weber and R. K. Chakravorti, *J. Am. Inst. Chem. Eng.*, **20**, 228 (1974).
20. M. Chen, Y. Chen and G. W. Diao, *J. Chem. Eng. Data*, **55**, 5109 (2010).
21. H. M. Freundlich, *Colloid Capillary Chemistry*, **3**(12), 1454 (1926).
22. H. M. Freundlich, Z. *Phys. Chem.*, **57A**, 385 (1906).
23. L. Yuhan, L. Mingce, H. Peidong, C. Ya and H. Juwei, *J. Hazard. Mater.*, **264**, 195 (2014).
24. C. Xinqing, F. L. Koon and L. Y. King, *Chem. Eng. J.*, **172**, 728 (2011).
25. U. Irina, S. Alexandru and V. Aurelia, *J. Colloid Interface Sci.*, **377**, 184 (2012).
26. B. S. Liu, D. F. Xu, J .X. Chu, W. Liu and C. T. Au, *Energy Fuels*, **21**, 250 (2007).
27. C. Xinqing, A. Manuel and L. Y. King, *Catal. Today*, **204**, 140 (2013).
28. Z. Weijia, S. Z. Wenhe, W. Yingjun, Z. Hongshi, L. Zhengmao and Y. Shunpu, *J. Magn. Magn. Mater.*, **321**, 1025 (2009).
29. L. Yujin, S. Kunyan, L. Rongzhan, Z. Xin, Z. Yang, L. Hongchao and X. Yanzhi, *Energy Procedia*, **61**, 863 (2012).
30. S. Rengaraj, C. K. Joo, Y. Kim and J. Yi, *J. Hazard. Mater.*, **102**(2-3), 257 (2003).
31. J. Tang, Z. f. Yang and Y. J. Yi, *Procedia Environ. Sci.*, **13**, 2179 (2012).
32. Q. Meng, X. Zhang, C. He, P. Zhou, W. Su and C. Duan, *Talanta*, **84**, 53 (2011).
33. H. Ruihua, L. Qian, H. Jie and Y. Bingchao, *Arabian J. Chem.* (2013), DOI:10.1016/j.arabjc.2013.05.017.
34. T. Fang-Chang, M. Ning, C. Tai-Chin, T. Lung-Chang, S. Jing-Jing, A. Yue Xia, T. Jiang, S. Shuenn-Kung and C. Fu-Sheng, *J. Water Process Eng.*, **1**, 2 (2014).
35. L. Tonghao, L. Yanhui, D. Qiuju, S. Jiankun, J. Yuqin, Y. Guangming, W. Zonghua, X. Yanzhi, Z. Wei, W. Kunlin, Z. Hongwei and W. Dehai, *Colloids Surf., B: Bio Interfaces*, **90**, 197 (2012).
36. Y. Yunjin, H. Bing, X. Feifei and C. Xiaofeng, *Chem. Eng. J.*, **170**, 82 (2011).